New frontiers in supramolecular design of materials

Samuel I. Stupp* and Liam C. Palmer

The powerful functions of materials in the living world utilize supramolecular systems in which molecules self-assemble through noncovalent connections programmed by their structures. This process is of course also programmed by the nature of the chemical environment in which the structures form introducing the potential to autonomously use external energy inputs partly derived from fuel molecules. Our laboratory has focused over the past three decades on integrating this notion of bioinspired supramolecular engineering into the design of novel materials. We present here three projects on functional supramolecular materials that address important societal needs for our future. The first is inspired by the photosynthetic machinery of green plants, creating materials that harvest light to produce fuels for sustainable energy systems. The second example is that of life-like robotic materials that imitate living creatures and effectively transduce different types of energy into mechanical actuation and locomotion of objects for future technologies. The third topic is supramolecular biomaterials that mimic extracellular matrices and provide unprecedented bioactivity to regenerate tissues to achieve longer "healthspans" for humans. In this example, we discuss a recent breakthrough in the structural design of supramolecular motion, which surprisingly led to biomaterials with the potential to reverse paralysis by repairing the brain and the spinal cord.

Introduction

This article is a summary of the 2022 Von Hippel Award talk given by Samuel I. Stupp at the Materials Research Society Fall Meeting & Exhibit. It is not meant to be a review on the subject of *Supramolecular Materials*, but it is rather a summary of topics covered in the talk based on previous work in the Stupp Laboratory at Northwestern University that led to the Von Hippel Award.

Since the pioneering work of Pedersen, Cram, and Lehn recognized by the 1987 Nobel Prize in Chemistry, supramolecular chemistry, which focuses on chemistry beyond the molecule, has greatly expanded to the development of a wide range of functional materials. Supramolecular materials are of course created with molecules, but the design of their components is based on specific noncovalent interactions across scales, including hydrogen bonds, π–π stacking, metal–ligand interactions, electrostatics, dipolar interactions, and steric forces, among others. Molecular design then programs the formation of functional structures in a specific chemical environment aided as needed by external energy inputs. The platform of supramolecular materials has elements of self-assembly, but it is by no means the autonomous process utilized by biological systems developed over billions of years of evolution. The platform can lead to superstructures and hierarchical materials that have the potential to emulate or perhaps rival those found in the biological world. Also, the tunability of noncovalent bond energies provides the opportunity to design highly dynamic materials that could imitate the motions of living creatures, adapt to environments, or rapidly sense and deliver signals. Furthermore, supramolecular materials are now emerging that integrate inorganic phases or covalent polymers to enhance mechanical robustness, add functions, and provide processing advantages. Biology uses this concept in some of its remarkable materials, such as cell membranes, the cytoskeleton, muscles, and bones. Given the enormous structural space available for the design of supramolecular materials, the field will benefit greatly from rapidly developing machine learning strategies, new theories, and large-scale computer simulations.

In 1997, the Stupp laboratory reported on the development of mushroom-shaped, noncentrosymmetric zero-dimensional

Samuel I. Stupp, Simpson Querrey Institute for BioNanotechnology, Northwestern University, Chicago, USA; Department of Chemistry, Northwestern University, Evanston, USA; Department of Biomedical Engineering, Northwestern University, Evanston, USA; Department of Materials Science and Engineering, Northwestern University, Evanston, USA; Department of Medicine, Northwestern University, Chicago, USA; s-stupp@northwestern.edu
Liam C. Palmer, Simpson Querrey Institute for BioNanotechnology, Northwestern University, Chicago, USA; Department of Chemistry, Northwestern University, Evanston, USA; liam-palmer@northwestern.edu
*Corresponding author
doi:10.1557/s43577-024-00669-x

nanostructures.[1] The nanostructures were formed by rod-coil monomers based on a short flexible styrene/isoprene diblock polymer coil covalently conjugated to a crystallizable rod-like biphenyl ester segment (**Figure 1**a). Attractive interactions among rod segments led to nanoscale crystallization of the monomers into fairly monodisperse nanostructures containing about 100 molecules. Small-angle electron diffraction (ED) shows the nanostructures form an oblique planar superlattice with a characteristic angle of 110°, while wide-angle ED patterns show that the nanostructures are crystalline. The resulting noncentrosymmetric polar nanostructures were on the order of 5 nm in size and organized into superlattices. Molecular dynamics (MD) simulations revealed that at larger aggregation numbers, the coils become conformationally restricted, which suggested that the finite crystallization into zero-dimensional nanostructures is entropically limited.[2]

Interestingly, these mushroom-shaped nanostructures further assembled into layers with polar ordering, and their macroscopic films were shown to have measurable piezoelectricity[3] and second-harmonic generation from infrared photons. The plastic-like films formed by layers of the mushroom-shaped nanostructures also exhibited hydrophobic and hydrophilic opposite surfaces as a result of polar ordering and thus resembled a self-assembled adhesive tape containing a nonadhesive surface.

In the context of hybrid materials composed of covalent and supramolecular polymers, we discovered systems in which a highly ordered membrane developed when a dilute solution of positively charged supramolecular peptide amphiphile (PA) nanofibers came into contact with a dilute solution of negatively charged hyaluronic acid, a high molecular weight biopolymer (Figure 1b).[4] A diffusion barrier rapidly forms at

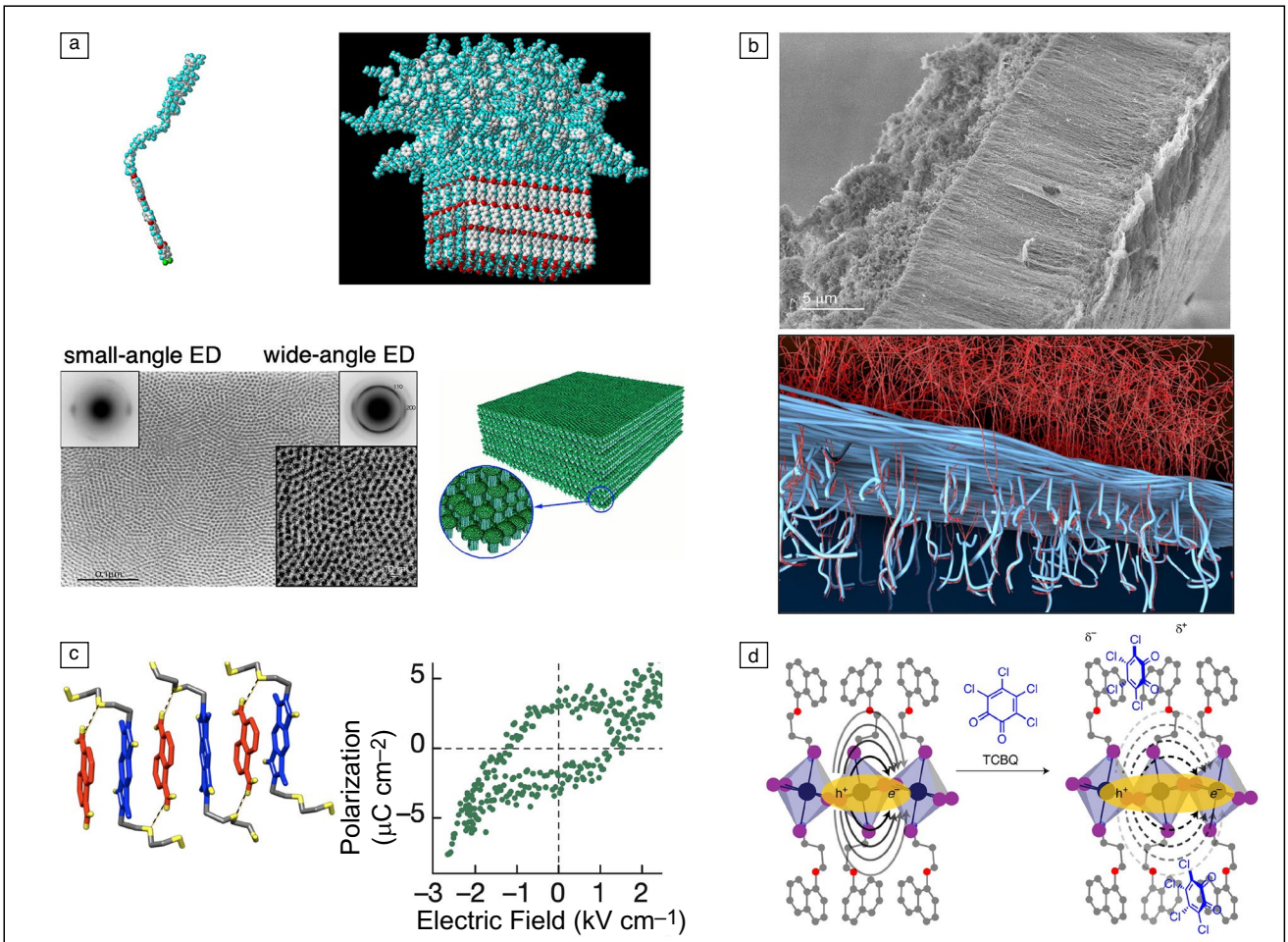

Figure 1. (a) Top: Molecular graphics representation of rod-coil molecules and their assembly into a mushroom-shaped nanostructure. Bottom left: Electron micrograph and electron diffraction (ED) patterns with the 110 and 200 indices labeled (inset). Bottom right: Schematic polar ordering of the mushroom assemblies. (b) Top: Scanning electron micrograph of a hierarchical membrane after 30 min (hyaluronic acid (HA) solution side on top, peptide amphiphile (PA) solution side on bottom). Bottom: Schematic representation of polymer (red) penetrating the diffusion barrier. (c) Molecular graphics representation of a complex between pyromellitic diimide-based electron acceptor and an electron-rich tetrathiafulvalene (TTF) derivative and associated room-temperature polarization hysteresis curves revealing their ferroelectric properties. (d) Schematic of the $n = 1$ layered perovskite upon doping with tetrachloro-1,2-benzoquinone (TCBQ) (blue molecule). Carbon, oxygen, nitrogen, lead, and iodine atoms are shown in gray, red, blue, indigo, and purple, respectively. Reprinted with permission from References 1, 4, 9, and 14.

the interface between the solutions preventing the chaotic complexation of oppositely charged components. Instead, a membrane slowly grows thicker as osmotic pressure differences drive the polymer through the interfacial layer causing its uncoiling as it complexes with oppositely charged supramolecular assemblies, thus producing a highly ordered membrane with filaments parallel to the thickness of the membrane. Importantly, these hierarchical membranes do not form when the precursors are PA monomers that form spherical micelles rather than long filaments.[5] The thickness of these membranes and thus their permeability and mechanical properties can be tuned by the incubation time[6] or by the application of an electric field.[7]

Our group has also explored crystals formed by stacks of electron donor and electron acceptor molecules that create ferroelectric materials as a result of charge transfer between them and the formation of ordered dipole moments. Previous studies on such stacks had reported ferroelectric properties at cryogenic temperatures (81 K).[8] Inspired by this work, we first reported in 2012 that designing specific intermolecular hydrogen bonds between the molecules engaged in charge–transfer interactions can stabilize broken symmetry and create ferroelectric materials at room temperature.[9,10] Specifically, the electron-poor acceptor consisted of a pyromellitic diimide functionalized with diethylene glycol chains that could interact with electron-rich donors based on naphthalene, pyrene, or tetrathiafulvalene (Figure 1c). The three supramolecular networks reported showed ferroelectric hysteresis at 300 K. In a follow-up study, we reported a related charge-transfer system in which the acceptors and donors crystallize in a 2:1 ratio with polarization hysteresis along both the face-to-face and edge-to-face axes.[11] The noncentrosymmetric nature of the molecular packing was confirmed by second-harmonic generation measurements. Supramolecular design offers a great deal of modularity because many different donors and acceptors can be synthesized using similar supramolecular motifs.

Hybrid organic–inorganic perovskites with the general chemical formula R-NH_3PbI_4 have attracted great interest for their use in high-efficiency photovoltaic devices, but they suffer from poor chemical stability.[12] In a subset of these materials, known as $n = 1$ layered perovskites, the fundamental PbI_6 octahedra are confined to two-dimensional layers that alternate with organic ammonium cations. The confinement of the semiconductor to two dimensions separated by low dielectric organic cations raises the bandgap and exciton binding energy, allowing the possibility for bandgap tuning and the development of emissive materials. However, these materials tend to orient with the inorganic layers parallel to the substrate, which results in low out-of-plane conductivity and compromises the photovoltaic performance in these otherwise environmentally stable materials. To improve the out-of-plane conductivity in these materials, we designed perovskite materials using R-NH_3I ammonium salts where R is a large aromatic moiety such as naphthalene, pyrene, or perylene.[13] Single crystals of the perylene and pyrene perovskites displayed conductivity that was several orders of magnitude higher than perovskites formed from typical aliphatic ammonium cations. We later reported that we could tune the 1 s exciton binding energies in electron-rich $n = 1$ perovskites by doping with electron-poor small molecules.[14] Specifically, we found that tetrachloro-1,2-benzoquinone (TCBQ) could engage in charge–transfer interactions with aromatic moieties in the perovskite, resulting in screening of the exciton and a lower binding energy without significant disruption to the inorganic lattice (Figure 1d).

Light-harvesting materials to generate solar fuels

Supramolecular systems that contain chromophore moieties offer a path to creating materials that can use the energy in visible light to perform useful chemical transformations. For example, our group has reported on several examples of chromophore amphiphile (CA) molecules that can assemble into light-absorbing supramolecular hydrogels.[15] The inspiration for these materials comes from the chloroplasts of plant cells, in which assemblies of chromophores transform visible light into chemical energy. The precise spatial positioning of chromophores within these supramolecular assemblies facilitates the formation of excitons and facilitates charge transport. Importantly, for their potential photocatalytic function, these hydrogels also have the capacity to harvest light and bind catalysts, as well as creating fluid compartments that promote diffusion or reactive precursors and products.

Light-harvesting supramolecular filaments

In an early example reported in 2014, we discovered photocatalytic supramolecular materials formed by self-assembly of visible light-absorbing perylene monoimide (PMI) amphiphiles.[15] In this work, we showed that PMI-containing molecules assemble into ribbon-like nanostructures in water through attractive π–π stacking and antiparallel dipolar interactions that compete with electrostatic repulsion among the carboxylate headgroups (**Figure 2**a–b). Solutions were prepared by suspending CAs in water with 1 equivalent NaOH to deprotonate the carboxylic acid headgroups at room temperature. Interestingly, when the repulsive electrostatic interactions were screened with salt, the samples showed a strong shift in the absorbance to both the red and blue, which was not easily attributed to typical H- or J-aggregation (Figure 2c). Synchrotron wide-angle x-ray scattering revealed sharp Bragg peaks, indicative of a high degree of internal molecular order (Figure 2d).[15,16] These negatively charged supramolecular assemblies, in turn, assembled into highly hydrated hydrogels in the presence of additional screening ions, such as divalent cations (e.g., Ca^{2+}) or polyelectrolytes (e.g., poly(diallyldimethylammonium chloride)). Given the strong light absorption properties of these hydrogels, we explored their use as photosensitizers for a nickel-based H_2 evolution catalyst. Supramolecular design was utilized here by selecting ligands for Ni ions bearing positive charge, thus electrostatically attracting the catalyst to the light-harvesting filaments

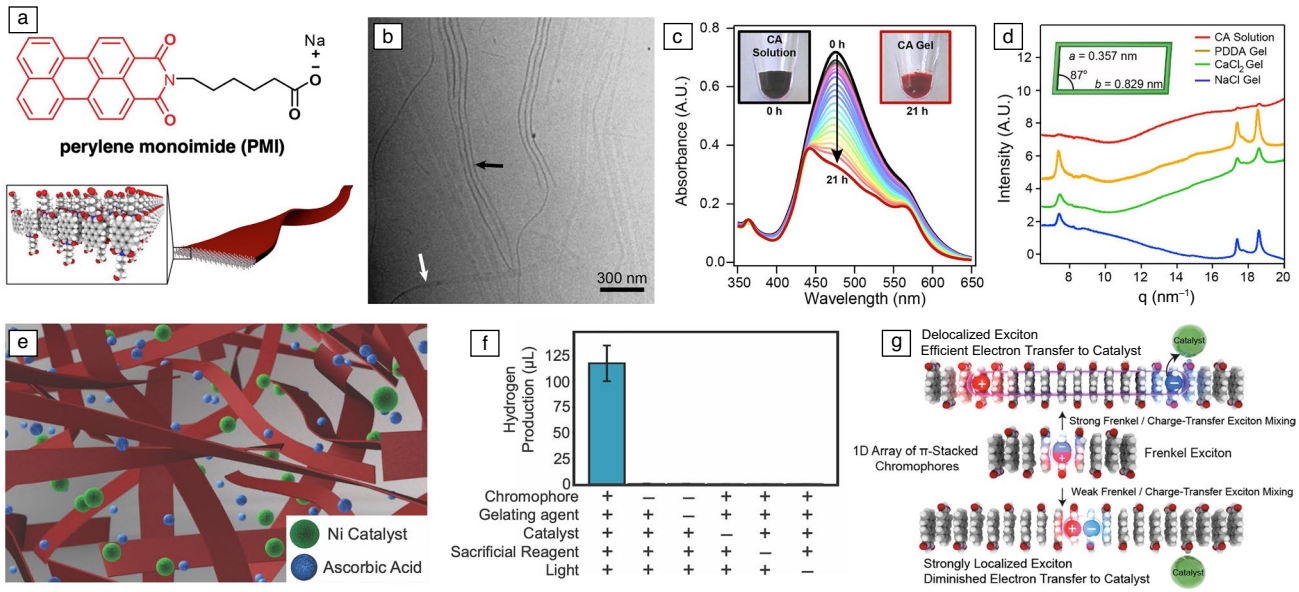

Figure 2. (a) Molecular structure and space-filling model of PMI-based chromophore amphiphile (CA). (b) Cryogenic transmission electron microscopy micrograph of CA solution reveals 40-nm-wide supramolecular ribbons. Differences in contrast arise from imaging a ribbon either face on (white arrow) or edge on (black arrow). (c) Absorbance spectroscopy shows changes in light absorption concomitant with gelation by poly(diallyldimethylammonium chloride) (PDDA) over 21 h. (d) Wide-angle x-ray scattering profiles for aqueous CA solutions gelled with PDDA, $CaCl_2$, or NaCl showing peaks at 7.3, 17.3, and 18.5 nm^{-1} that correspond to a 2D distorted rectangular lattice (inset). (e) Schematic of gel of CA nanoribbons (red) with room for diffusion of water and reagents. (f) H_2 evolution experiments show that the gel can photosensitize a nickel catalyst for H_2 evolution; H_2 was not evolved without chromophore, catalyst, sacrificial reagent, or light. (g) Graphical illustration of Frenkel excitons (FEs) and charge-transfer excitations (CTEs) in PMI systems. A FE localized at $n = 0$ (top left corner) can directly couple to a variety of FE and CTE states. Reprinted with permission from References 15 and 17. © 2014 Nature Publishing Group and © 2016 American Chemical Society.

(as shown schematically in Figure 2e). In the context of natural photosynthetic systems, the use of noncovalent interactions offers a strategy to localize all the necessary components required for the photocatalytic production of molecules. Irradiation of solutions of the CA gels with the catalyst and ascorbic acid as a proton source and sacrificial electron donor showed production of H_2, while no H_2 evolution was observed in control experiments in which CA, ascorbic acid, or catalyst was omitted from the system (Figure 2f). Computational studies with the Spano Laboratory showed that crystalline packing within these nanostructures could support coupled molecular Frenkel excitations (FEs) and charge-transfer excitations (CTEs), leading to longer exciton lifetimes (Figure 2g). These results were consistent with the observed spectra and greater H_2 production was observed in systems predicted to have more FE/CTE mixing and better spectral overlap with the wavelength of incident photons.[17]

We also found that the assembly pathway had an important effect on nanoscale structure and photocatalytic performance.[18] Annealing the same PMI CAs at 95°C for 1 h under high ionic strength (50-μM NaCl) leads to the growth of wide ribbon-like crystalline assemblies that are 1–10-μm long, 100 s of nanometers wide, and the thickness of one layer of interdigitated molecules (**Figure 3**a–b).[19] Using a combination of solution WAXS, grazing incidence WAXS (GIWAXS), TEM, and selected-area electron diffraction studies, we found that the direction of π–π stacking ran parallel to the long axis of the supramolecular polymer. Importantly for efficient excitonic transport, the diffraction spots, and the lack of reflections at the same radii indicated that the supramolecular polymers are single-crystal-like in nature and that their domains align along the same axis (Figure 3c). Interestingly, SEM images revealed aligned rectangular holes throughout the supramolecular polymers, where monomers were chemically extracted with ethanol and supercritical carbon dioxide during the critical point drying (Figure 3d). Scanning electron micrographs of dried hydrogels showed a highly porous network when the extra-large crystalline supramolecular polymers were used relative to those formed from control samples (Figure 3e–f). The resulting highly crystalline and highly porous materials showed enhanced photocatalytic hydrogen production with turnover numbers for H_2 production as high as 13,500 over ~110 h compared to only 7500 for materials prepared from smaller, more densely packed structures (Figure 3g).

Subsequent work revealed that the assembly morphology and photocatalytic turnover depended strongly on the molecular structure. For example, the length of the linker between the aromatic chromophore and the carboxylic acid headgroup had a strong effect on photocatalysis, with maximum turnovers with a five methylene linker, which gave a nanoscale morphology and molecular packing arrangement that was well suited for intermolecular HOMO–HOMO orbital overlap and better excitonic splitting.[20] Incorporation of an electron-withdrawing group (cyano) on the aromatic

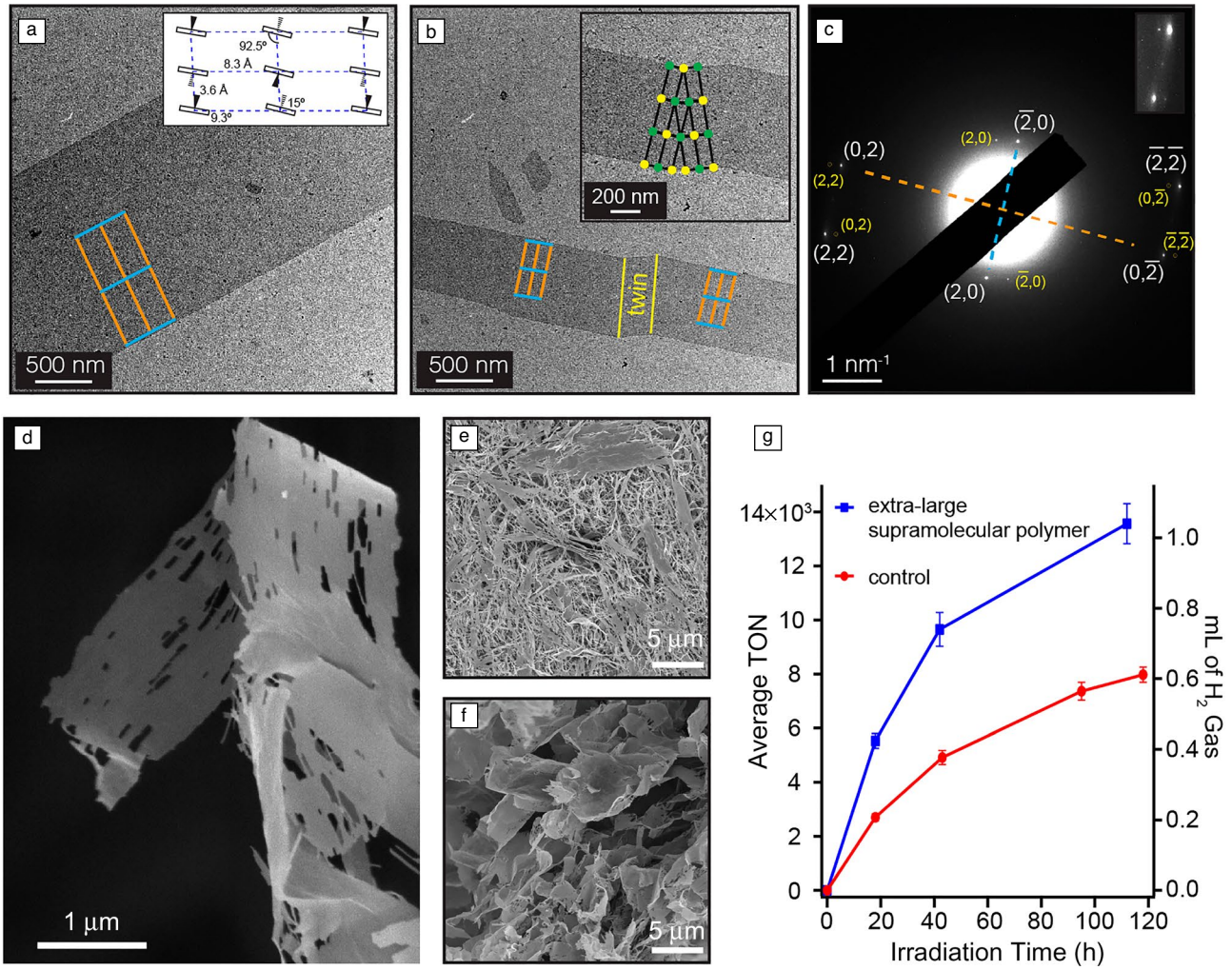

Figure 3. (a) Transmission electron microscopy (TEM) image of a single supramolecular polymer ribbon formed from the PMI CA after heating to 95°C for 1 h followed by slow cooling; inset shows the schematic of a unit cell of the supramolecular polymer derived from wide-angle x-ray scattering data, with the carboxylate group orientation indicated by the wedges (the orange and blue lines show the (01) and (10) edges of the lattice in the inset). (b) TEM image of a single supramolecular polymer containing twin boundaries; the inset shows a magnified view of the twinned region. (c) Indexed selected-area electron diffraction pattern of the supramolecular polymer in panel b; inset shows a magnified view of the (02) and (22) diffraction spots. (d) Scanning electron microscopy (SEM) image showing an extra-large supramolecular polymer in which the monomer was extracted by ethanol after annealing, leaving behind rectangular crystal holes with a common orientation; micrograph reveals the single-crystal-like morphology of the supramolecular polymer. SEM images of gels formed from the unannealed control PMI CAs (e) or the annealed PMI CAs that create the extra-large supramolecular polymers (f). (g) Turnover number (TON) as a function of time for H_2 production using $Na_2[Mo_3S_{13}^{2-}]$ clusters as the catalyst within hydrogels composed of extra-large supramolecular polymers and an unannealed control. Reprinted with permission from Reference 19. © 2021 American Chemical Society.

ring lowers the net dipole moment and reduces the driving force for assembly, whereas an electron-donating group (amino) has the opposite effect.[21] However, the unsubstituted aromatic ring (with an intermediate dipole moment) gave the greatest charge-transfer exciton formation and the highest photocatalytic hydrogen evolution. Adding bulky "tail" to the aromatic core was found to weaken the driving force for assembly.[22] Despite the steric bulk a PMI with a 3-pentylamino substituent displayed a strongly red-shifted absorbance band and enhanced hydrogen evolution relative to the other alkyl amine tails investigated. Using these different substituents, we uncovered a strategy to make multicomponent PMI supramolecular materials, inspired by alloying approaches commonly used in metallurgy. In this study, we confirmed the formation of supramolecular alloys using x-ray scattering, microscopy, and optical spectroscopy (**Figure 4**a).[23] Furthermore, compositional variations led to changes in the physical, photophysical, and mechanical properties of these materials, in addition to the formation of a crystalline phase consisting of multiple molecular species analogous to intermetallic compounds. We were also able to use the thermal stability of the crystalline pure phases to create seeds for size-controlled supramolecular polymerizations (Figure 4b). This metallurgy-inspired approach provides

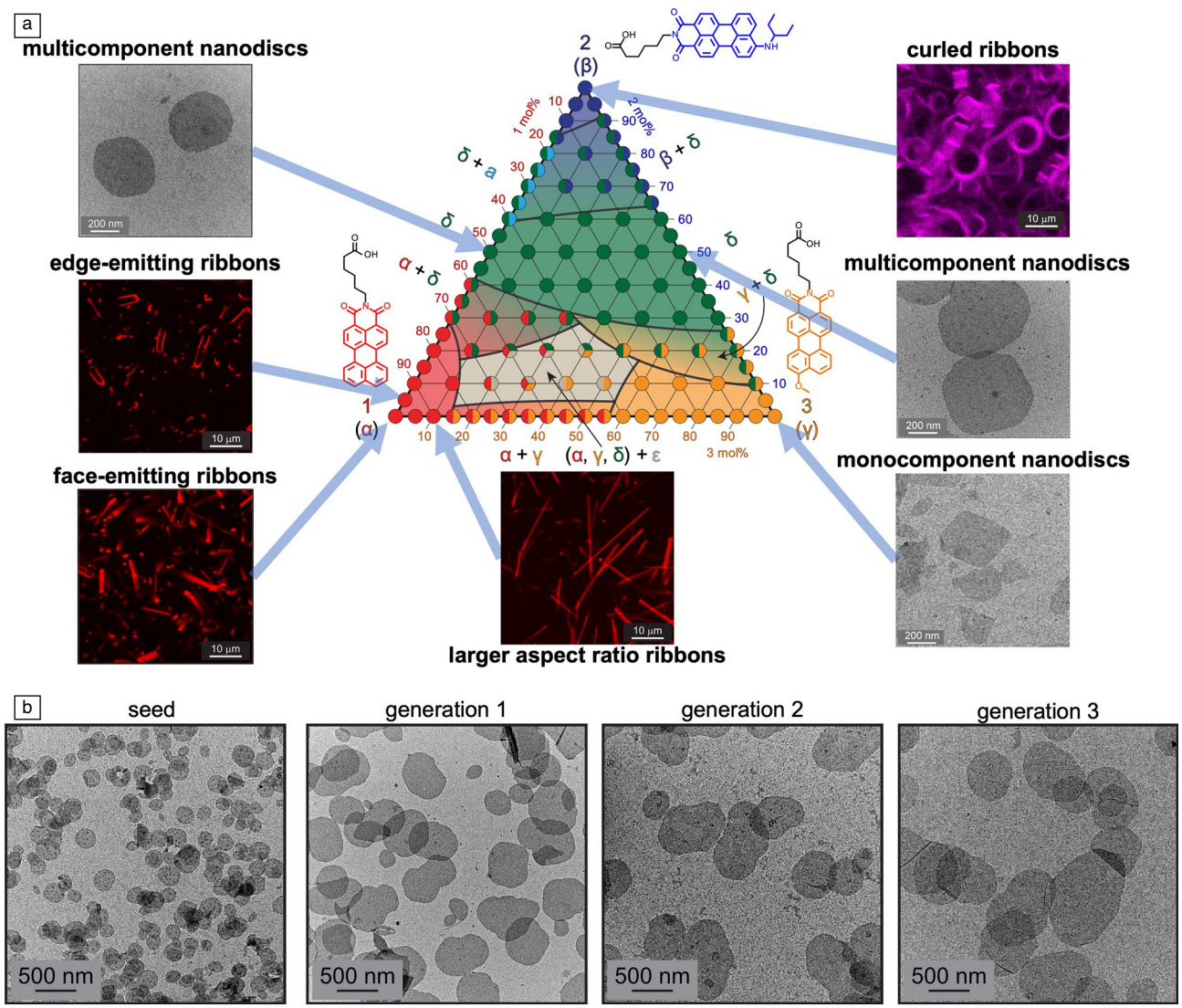

Figure 4. (a) Ternary phase diagram of PMIs **1**, **2**, and **3** in various molar ratios after annealing for 1 h at 95℃ (colors indicate the dominant phase; red, α-phase; dark blue, β-phase; light blue, amorphous assemblies of PMI **2**; orange, γ-phase; green, δ-phase; gray, mixed regions). (b) Transmission electron microscopy images of δ-phase nanodiscs at various stages of living polymerization. Reprinted with permission from Reference 23. © 2023 Cell Press. The micrograph of the curled nanoribbons is reprinted from Reference 24. © 2020 American Chemical Society.

access to unique structures and properties that are not simply linear combinations of the constituent components.

Hybrid bonding polymers

We recently defined the term hybrid bonding polymers (HBPs) to refer to systems "in which the constituent monomers are designed to polymerize noncovalently or covalently and have structures that enable rational chemical integration between the supramolecular and covalent components."[25] A recent example of this concept can be found in our recent report on a strategy in which PMI CA small molecules integrate with a disordered polymer (poly(ethylene-*alt*-maleic anhydride, PEAMA) functionalized with pendant PMI moieties (**Figure 5**).[26] Cocrystallization of the common PMI segments led to an ordered lattice of light-harvesting assemblies "jacketed" by conformationally disordered charged polymer backbones that provide solubility in water, as revealed by synchrotron x-ray scattering, absorption spectroscopy, and coarse-grained MD simulations (Figure 5a–g). The morphology of this HBP nanostructure is determined by competition between the enthalpy of the crystalline lattice and the polymers' entropy. We observed that the hybrid nanostructures exhibit higher fracture strength and the capacity for self-healing, which increases their utility for applications, such as light harvesting and photocatalysis (Figure 5h).

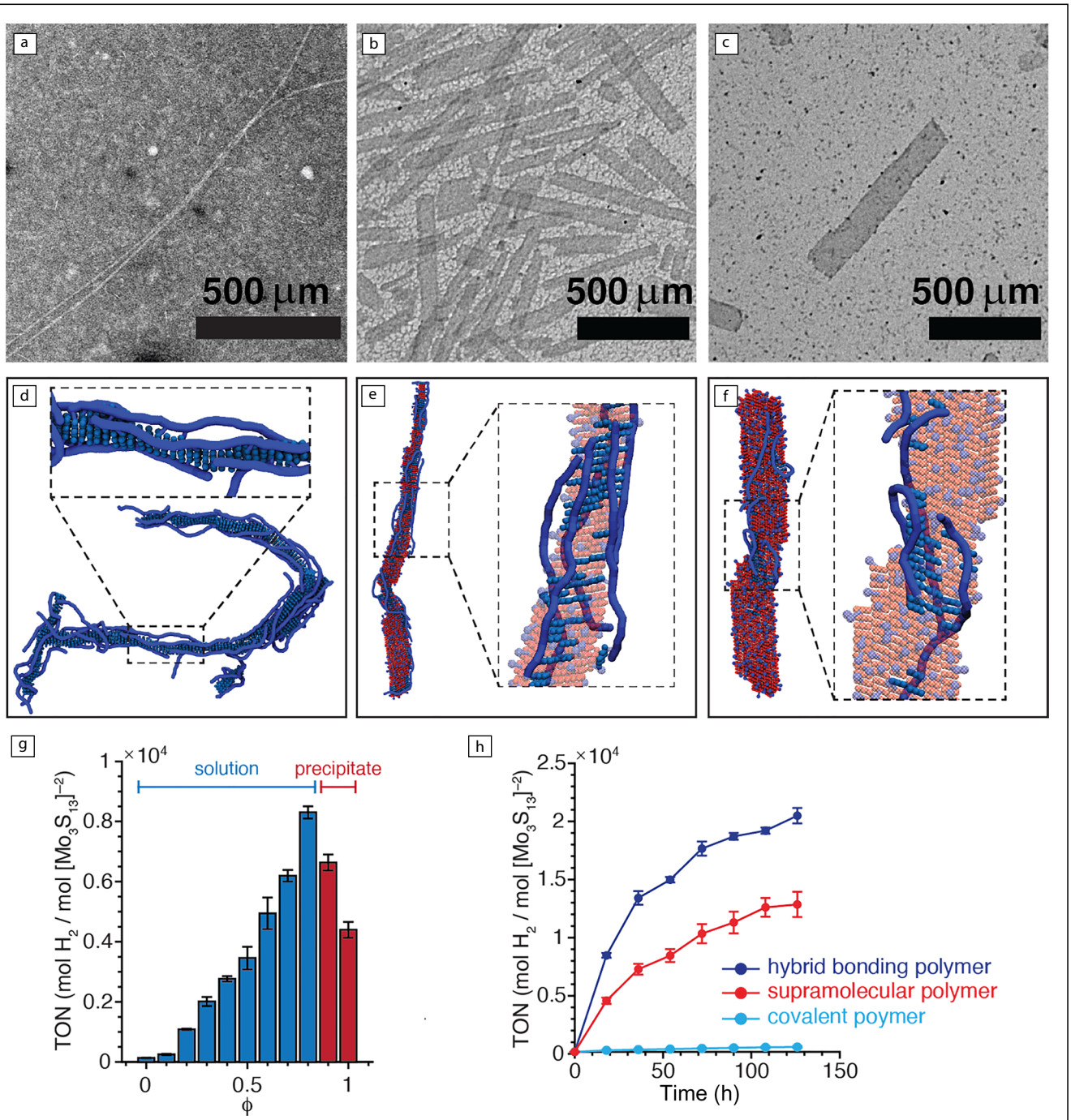

Figure 5. (a–c) Representative conventional transmission electron microscopy micrographs of the hybrid bonding polymers (HBPs) with co-assembly ratios $\phi = 0$ (a), 0.7 (b), and 0.9 (c), where ϕ is defined as the fraction of PMI chromophores in CA small molecules versus the total number of PMIs in the system. Scale bars are 500 nm. (d–g) Snapshots from the coarse-grained molecular dynamics simulations of hybrid bonding polymers at $\phi = 0$ (e), 0.7 (f), and 0.9 (g), showing the presence of the exo-crystalline layer; the covalent polymer backbone is colored dark blue, the covalently bonded PMI chromophores are colored light blue, and the free PMI chromophores are colored red. (h) Turnover number (TON) of hydrogen produced with a thiomolybdate catalyst after 18 h of irradiation for HBPs with different values of ϕ. (i) TON values of the best performing HBP ($\phi = 0.8$), the supramolecular polymer ($\phi = 1.0$), and the covalent polymer ($\phi = 0$) as a function of time. Reprinted with permission from Reference 26.

Covalent–supramolecular hybrids as robotic materials

Inspired by many different aquatic nonvertebrate creatures such as cephalopods and jellyfish, synthetic soft matter offers an exciting opportunity to create materials that encode responsiveness to external stimuli and the potential for autonomous functionality. These materials could be useful for the design of artificial skeletal tissues or wire-free soft

robots. Some pioneering work in this area used photoactive liquid-crystalline elastomers to create films with periodic mechanical waves[7] and an artificial light-driven flytrap.[8] Given the highly dynamic nature of supramolecular polymers, we hypothesized they could have a very important role in the actuation of soft matter. Indeed, supramolecular structures play critical roles in biology, such as the assembly of cytoskeletal filaments, the dynamic interaction of cells through focal adhesions, and the contraction and expansion of muscle sarcomeres. Our scientific objective was to learn how to encode responsive behavior in materials through molecular and supramolecular design rather than by the direct application of external forces. In an early demonstration of this concept, we created macroscopic hydrogel tubes that reversibly contract and expand anisotropically with changes in temperature.[13]

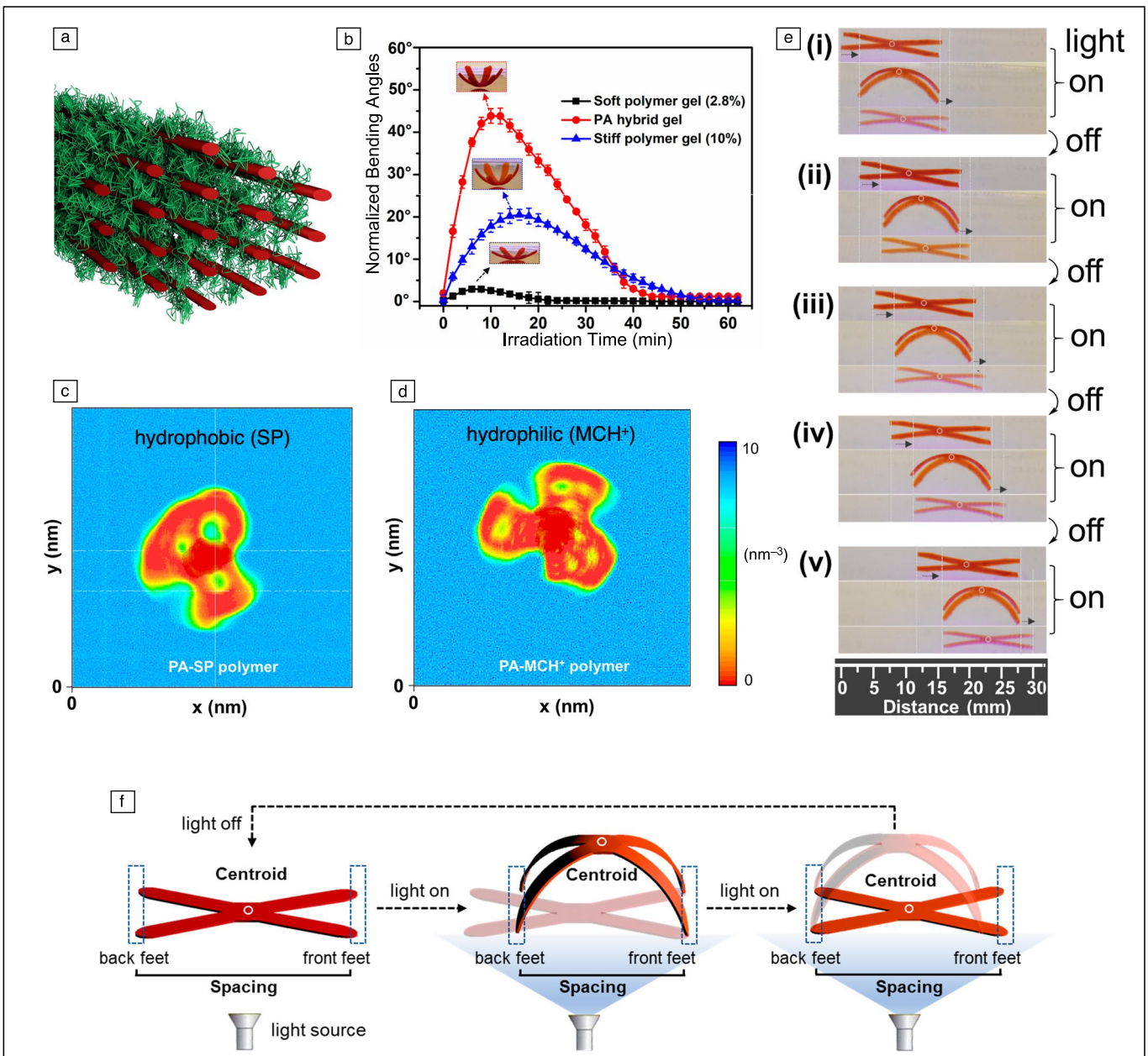

Figure 6. (a) Schematic of the bundle structure depicting the short-range alignment of supramolecular PA fibers (red) inside the network of covalent polymers (green). (b) Bending kinetics of PA hybrid films compared to polymer films with 2.8% or 10% cross-linker densities normalized for the total concentration of photoactive moieties (SP and MCH^+). Two-dimensional spatial distribution of water number density calculated by molecular dynamics simulations and averaged over the long axis of the PA supramolecular polymer (z-axis) for the PA–SP hybrid (c) and PA–MCH^+ hybrid (d). The shaded region in the center shows the position of the PA nanofiber as a 2D density distribution calculated in the same manner. (e) Photograph snapshots of five steps by the object moving from left to right by a bending and flattening process on a ratcheted PDMS surface after alternating light and dark periods. (f) Schematic representation of the crawler moving through sequential bending and flattening processes. Reprinted with permission from Reference 27. © 2020 Nature Publishing Group.

Encouraged by the reversible thermal actuation in these systems, we explored the potential for similar anisosoptric actuation in materials that respond to light. To this end, we developed a hybrid hydrogel containing PA supramolecular polymers bonded chemically to a covalent network containing spiropyran photoswitches (**Figure 6**a).[27] These moieties could be switched between two distinct chemical structures using light, a charged hydrophilic open form (merocyanine, MCH^+) and a noncharged hydrophobic form (spiropyran, SP). Upon irradiation with visible light, films of the covalent spiropyran polymers exhibited reversible contraction to about 84% of the original size, due to differences in hydration of the MCH^+ and SP moieties. Interestingly, incorporating PA supramolecular polymers into the network led to a similar extent of shrinkage, but greatly accelerated the process. Films of these materials were found to display bending actuation and crawling motion under the influence of light, and both computational and experimental work helped us understand the critical functional roles of the supramolecular assemblies. In particular, films with star-shaped geometries reversibly bend toward a light source to a much greater extent than similar films prepared using only covalent polymers (Figure 6b). Coarse-grained MD simulations revealed that the SP hybrids collapse around the PA nanofiber yielding a more continuous network that is segregated into two regions (Figure 6c). In contrast, the MCH^+ hybrids remain relatively extended with more space occupied by water molecules between the chains due to the hydrophilic nature of the MCH^+ isomer (Figure 6d). The volume occupied by the MCH^+ hybrid is larger than that of the SP hybrid, which helps explain our macroscopic observation that the hybrid hydrogel swells in the dark and contracts under the light. The simulations also suggested that the hydrophilic supramolecular nanofibers can help channel water out of the hydrogel, enhancing the overall speed of photoactuation.

We found that four-arm flat films of the PA hybrid hydrogel containing MCH^+ moieties bend toward a light source, which we interpret to be the result of a contraction gradient along the direction of light propagation. As light penetrates the film, the hydrophilic MCH^+ groups are converted to the more hydrophobic SP form, causing expulsion of water and local shrinkage of the hybrid material. The gradient-induced bending of these objects was found to be reversible because further illumination eliminates the gradient in mechanical contraction as the MCH^+ moieties are converted to SP. Figure 6f illustrates the unidirectional motion of a four-arm hydrogel "crawler" irradiated with a light source from below. The floor of the water tank had a ratcheted poly(dimethylsiloxane) (PDMS) surface to minimize slippage and enable unidirectional motion of the crawler. Under constant irradiation, the hybrid hydrogel crawler (16-mm long) containing supramolecular filaments moved from left to right approximately 2.2 mm over 30 min, whereas a similar object made up of a soft polymer gel without the supramolecular polymer moved forward only 0.5 mm over the same time (Figure 6e). We found that the irradiated crawler slowly expanded to its initial swollen size in the dark, preparing it for another light-induced crawling step. These results gave further evidence that the supramolecular reinforcement highly enhances light-driven actuation and enables longer distance movement of the crawler gel. Our vision is that supramolecular polymers can be used to encode a wide variety of motions and functions in soft matter, including walking, crawling, bending, twisting, rotating, and swimming. Furthermore, these materials could be designed to autonomously perform tasks to manage their environment.

Surprising bioactivity in supramolecular materials linked to dynamics

More than two decades ago, our group discovered a class of PAs that spontaneously self-assemble into 1D nanostructures in water.[28] The self-assembling PA molecule was based on a palmitoyl tail covalently linked to the N terminus of peptide sequences with a propensity to form a β-sheet secondary structure and electrostatic charge for solubility (**Figure 7**a). Hydrophobic collapse of the alkyl tails and hydrogen bonding interactions drive assembly into high-aspect-ratio nanofibers that are ~6–10 nm in diameter and up to micrometers long. These supramolecular nanostructures, which can display bioactive signals in high density on their surfaces, have shown great efficacy as extracellular mimetics and have revealed *in vivo* efficacy in models of spinal cord injury,[29,30] cartilage regeneration,[31] bone regeneration,[32] and vascular disease.[33] They collapse into networks of charged one-dimensional nanostructures when screened by electrolytes present in the physiological environment, and they are possibly the most bioactive biomaterials known due to their high signal densities and their biomimetic nature. Their biomimetic nature is based on the fact that natural extracellular matrices are largely composed of networks of filamentous supramolecular polymers in which proteins are the monomers as well as bundled conformationally ordered covalent polymers such as collagen (see Figure 7b comparing their architecture to natural matrices[34]). To better understand the relationship between peptide sequence and the morphology of supramolecular peptide nanostructures, we recently developed a model for PAs containing β-sheet forming domains that form twisted nanoribbons in water (Figure 7c).[35] In this model, the morphology emerges from a balance between energetically favorable packing of molecules in the center of the nanostructures, the unfavorable packing at the edges, and the deformations due to packing of twisted β-sheets. We also observed a change in the supramolecular chirality of the nanostructures as the peptide sequence was modified. With stronger electrostatic repulsion, we observed a change in morphology from long nanostructures to shorter rod-like fragments or spherical micelles.

Internal dynamics of supramolecular nanofibers

Our initial perspective on these nanostructures was to explore their static features, such as size, shape, and aspect ratio, which we could measure by techniques, such as electron

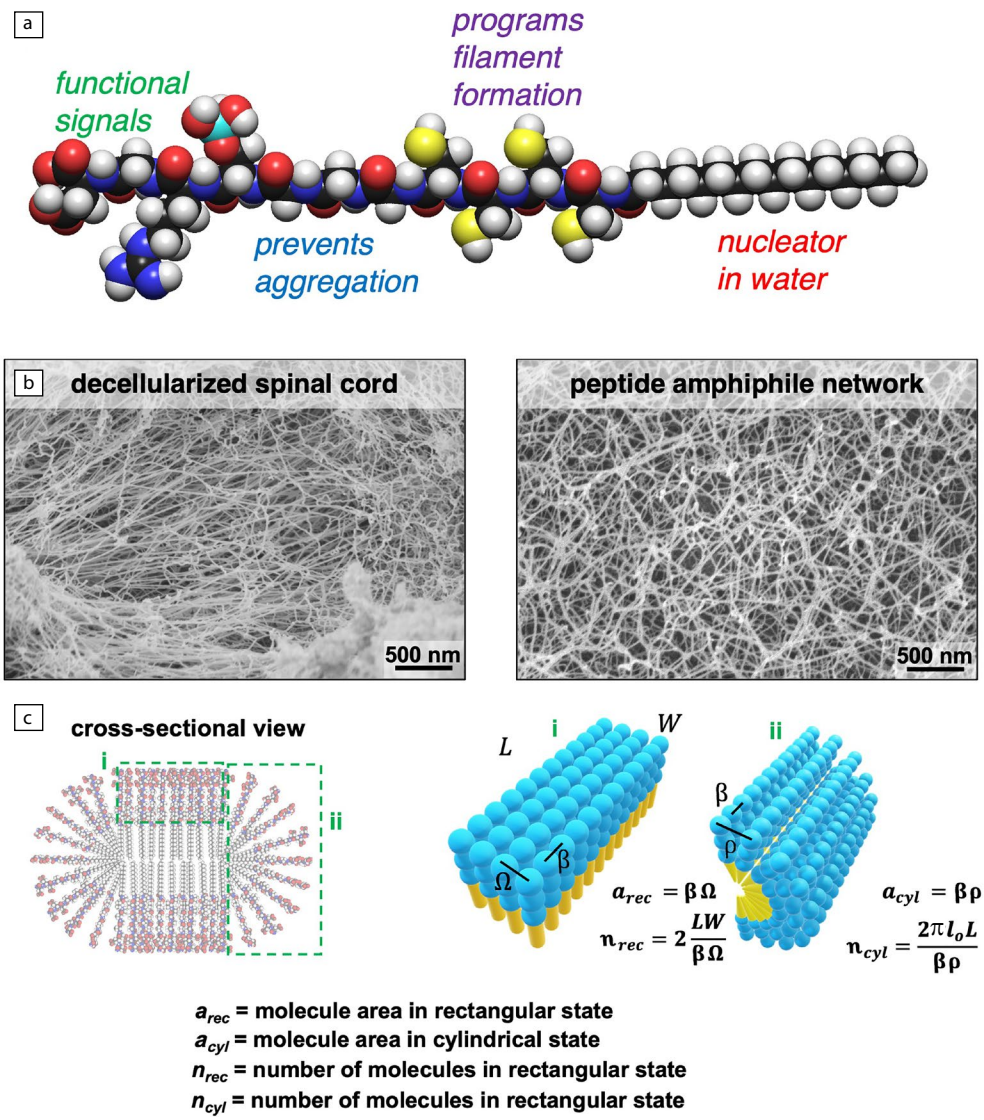

Figure 7. (a) Molecular graphics representation of PA molecule. (b) Scanning electron microscopy of decellularized spinal cord tissue (left) and the peptide amphiphile nanofiber network (right). (c) Left: Schematic representation of molecular self-assembly into nanostructures consisting of rectangularly packed center domains (i) and highly curved edges (ii). Right: Geometric model of PA assembly. β, Ω, and ρ are geometrical parameters of molecular spacing, *L* and *W* are morphological parameters for the length and width of the rectangular domain, and n_{rec} and n_{cyl} correspond to the number of molecules in rectangular and cylindrical domains, respectively. Reprinted with permission from References 34 and 35. © 2023 Cell Press and 2021 American Chemical Society.

microscopy and x-ray scattering. While these static characteristics certainly influence their functions, we more recently came to understand that it is also critical to consider the spatial dynamics of these supramolecular nanostructures. MD simulations are commonly used to access dynamics information on subnanometer length scales, but until recently experimental techniques have not been available that provide high spatial and temporal resolution on dynamics. We reported the first quantitative experimental study of conformational dynamics in a supramolecular polymer with subnanometer resolution.[36] Using electron paramagnetic resonance (EPR) spectroscopy, we investigated PA supramolecular polymers by incorporating radical electron spin labels at specific sites (**Figure** 8a). By performing quantitative EPR on nanofibers co-assembled with trace amounts of radical electron spin labels (0.4%), we identified dynamic behavior, which changed from liquid-like to solid-like and liquid-crystal-like across the ~7-nm cross section of the supramolecular PA nanofiber (Figure 8a). These measurements yielded rotational diffusion rates at the specifically labeled sites and revealed solid-like behavior in the interior of the nanostructures where there are high densities of β-sheet hydrogen bonds. This region becomes more dynamic when the nanofibers incorporate a methylated PA, which weakens the intermolecular hydrogen bonding. We also used a technique known as Overhauser dynamic nuclear polarization (ODNP) relaxometry,[37] which combines electron paramagnetic resonance (EPR) and ^{1}H nuclear magnetic resonance (NMR) spectroscopies and to capture events of translational diffusion of a water molecule as it passes by a radical electron spin label. This technique is thus well suited to measuring the hydration dynamics at different domains of the nanostructure. ODNP revealed that there were water molecules in the hydrophobic core and that water dynamics in this region were insensitive to gelation of nanofiber solutions with added calcium salts. In the peptide region near the core, water motion was found to be slower and this reduction in water dynamics was more pronounced in the gelled samples. When gelled with calcium ions, water at the nanofiber surface exhibited diffusion on the time scale of water that is physically confined within a protein cavity, while water molecules in solution samples

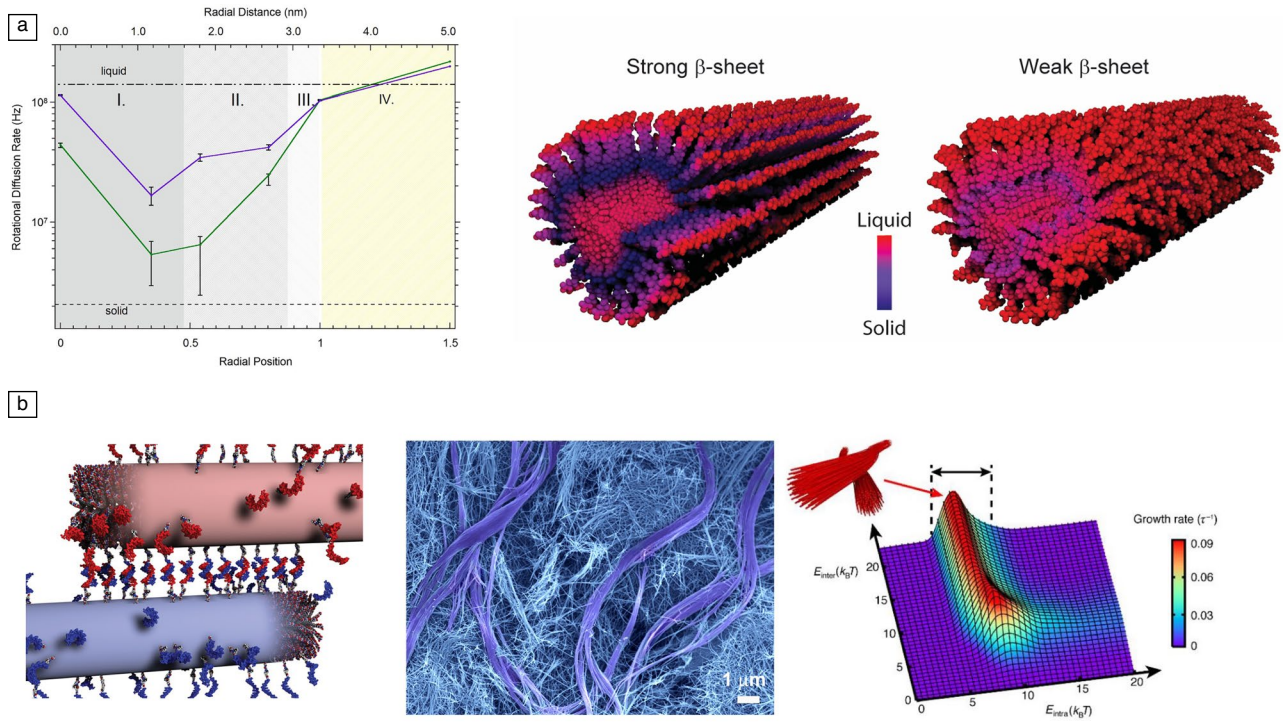

Figure 8. (a) Left. Plot of rotational diffusion rates calculated from electron paramagnetic resonance spectral simulations as a function of the theoretical radial position of the spin label at different positions in the nanofiber. Purple line corresponds to PA nanofibers designed to exhibit strong β-sheet character; green line corresponds to co-assemblies with weaker β-sheet character. The three domains of the nanofiber cross section are indicated as the aliphatic core (I), structural domain shell (II), and charged corona (III). Right. Schematic representation of the gradient of solid-like to liquid-like dynamics (blue and red, respectively) through the nanofibers' cross sections. (b) Left. Illustration of peptide amphiphile fibers cross-linked by DNA hybridization. Middle. Scanning electron microscopy micrograph of the hydrogel formed upon DNA cross-linking. Two populations within the gel are shown, consisting of twisted bundles (diameter ~1–3 mm) and single fibers (diameters 10–15 nm). Right. Bundle growth rate as a function of intra- and interfiber energies from coarse-grained molecular dynamics simulations. Bundles preferentially form within the energy range 5 $k_BT < E_{intra} < 10\ k_BT$ (black arrows). Reprinted with permission from References 37 and 38. © 2014 Nature Publishing Group and 2018 AAAS.

do not slow down as much. These ODNP studies revealed a remarkable variation in water dynamics between the fast-moving water in the hydrophobic core, to the slower, solid-like water at the hydrophilic surface, only a few nanometers away. These results, which were supported by atomistic MD simulations with explicit water, indicate that water dynamics can be an integral part of structure and function in hydrated materials.

Dynamic materials: Reversible hierarchical structures

Given the high degree of programmability and reversibility of interactions between complementary oligonucleotides, we were interested in exploring the use of these components to create dynamic, hierarchical materials. We decorated the peptide amphiphiles with single-stranded DNA using copper-free click coupling to an azide-containing PA. When we mixed an aqueous solution containing fibers with complementary oligonucleotides, we observed the expected formation of a gel that could be liquefied by adding a soluble single-stranded DNA that breaks the cross-links via strand displacement. SEM and fluorescence microscopy of these hydrogels revealed the apparent separation of large micrometer-sized bundles of fibers enriched with DNA within a network of individual DNA-depleted fibers (Figure 8b).[38] We hypothesized that extensive dynamic redistribution of monomers within and among the fibers was critical for the reversible formation of these hierarchical structures. Using CG-MD simulations, we found that dynamic molecular exchange over large spatial distances among the supramolecular assemblies is necessary to form the DNA-rich bundles. The model also allowed us to calculate the range of cohesion energies within assemblies that allow the transformation into the observed hierarchical structure (Figure 8b). We have also recently found similar reversible hierarchical bundling using electrostatic interactions among peptides[38,39] and using host–guest interactions.[40]

We very recently reported on a breakthrough to achieve central nervous system regeneration by controlling supramolecular dynamics in nanofibers formed by two molecules for cell signaling (**Figure 9**a–b).[29] We accomplished this by preparing PA supramolecular polymers containing two distinct signals. One signal activates the transmembrane receptor β1-integrin (IKVAV) and a second one activates the basic fibroblast growth factor 2 (FGF2) receptor. We hypothesized that the dynamics of molecules in the supramolecular materials in the extracellular space could greatly enhance the capacity

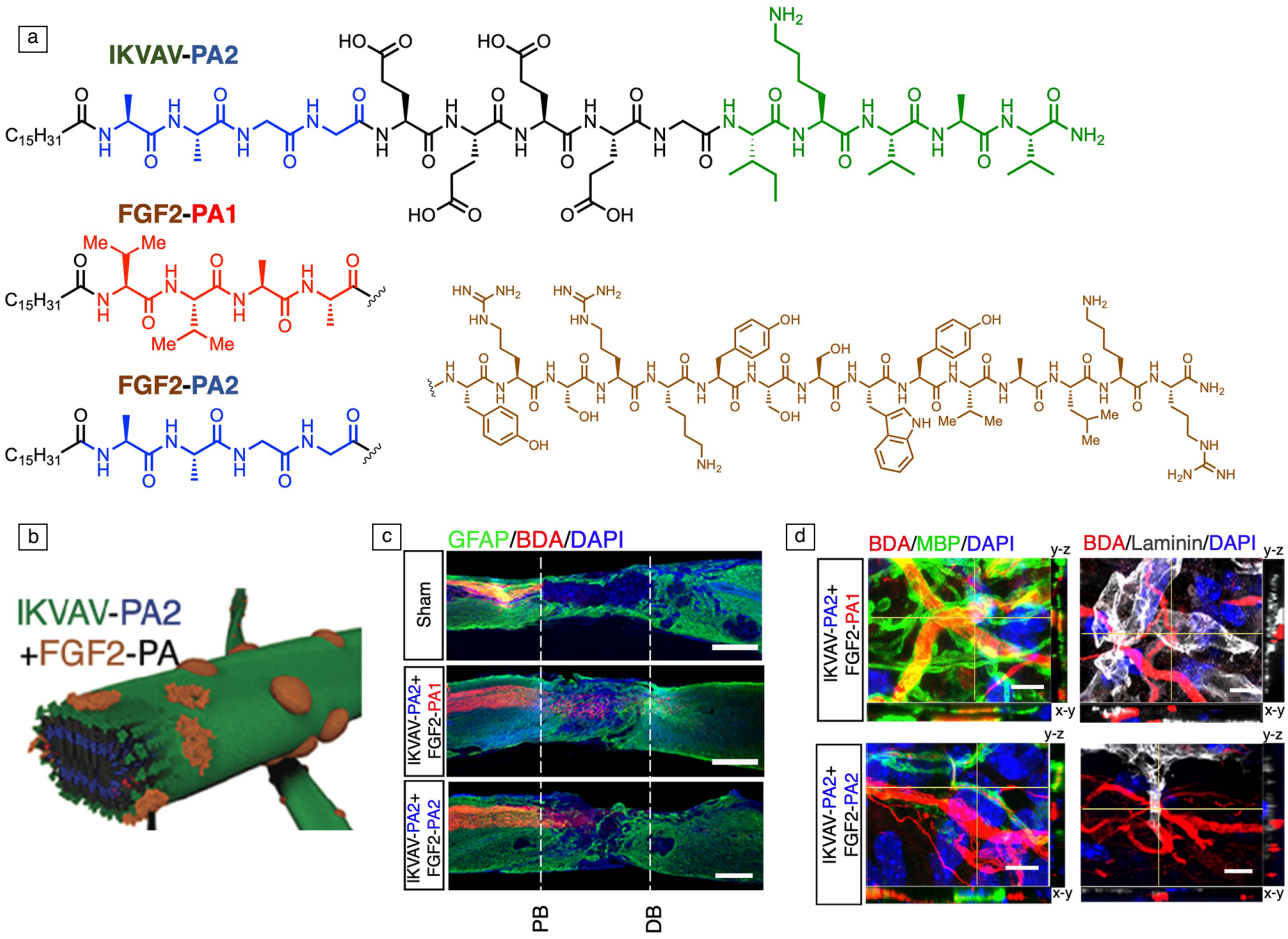

Figure 9. (a) Chemical structures of the PA molecules used (**IKVAV-PA2**, fast-moving **FGF2-PA1**, and slow-moving **FGF-PA2**). (b) Schematic representation of nanofiber containing 90-mol% **IKVAV PA** and 10-mol% **FGF2-PA1** or **FGF2-PA2**. (c) Fluorescence micrographs of longitudinal spinal cord sections in sham, **IKVAV-AP2**+**FGF2-PA1**, and **IKVAV-PA2**+**FGF2-PA2** groups. GFAP indicates astrocytes (green), BDA indicates labeled axons (red), and DAPI indicates nuclei (blue); vertical white-dashed lines indicate the proximal border (PB), the distal border (DB), and the central part of the lesion (LC). (d) Representative fluorescence micrographs of BDA-labeled axon regrowth (red) and myelin basic protein (MBP) (green) (left) and laminin (white) (right). Reprinted with permission from Reference 29. © 2023 AAAS.

of soft materials to signal cells. Indeed, mutating the peptide sequence of the amphiphilic monomers led to enhanced molecular motions within scaffold fibrils, as shown by NMR and fluorescence depolarization experiments and simulations. An *in vivo* model of severe spinal cord injury, we observed notable differences in vascular growth, axonal regeneration, myelination, survival of motor neurons, reduced gliosis, and functional recovery (Figure 9c–d). We are still trying to elucidate the ways that molecules move and exchange within these assemblies for enhanced bioactivity, but one interesting possibility is that they partially escape from supramolecular assemblies driven by low internal cohesion and entropic sampling of multiple interactions among domains of the molecules.[41]

Future outlook and concluding remarks

Supramolecular materials, in which functions are designed using our rapidly advancing knowledge about intermolecular interactions, are effectively the future of functional soft matter. This statement is justified by the fact that their structures and functions can be simultaneously designed by considering how molecules interact through nonprimary bonding. The exciting properties that could emerge would be transformative in materials science and engineering because they could cover not only conventional areas, such as mechanics, dynamics, and optical/electrical/magnetic behavior, but also properties of importance to our future, such as the lifecycle of soft materials and the ability to interface well with living organisms. On the structural side, we will gain the capacity to design hierarchical structures, which is central to the amazing functions of soft materials manufactured by nature. Furthermore, the platform of supramolecular materials can also integrate inorganic phases and covalent polymers to achieve an even greater scope of combined properties. The integration with inorganic phases is particularly important at the nanoscale, as interesting materials could emerge when structures such as quantum dots and others that are effectively "inorganic molecules" could be

rationally connected to organic components using noncovalent interactions. The integration of purely supramolecular phases, in which components are rationally connected via nonprimary bonds, to conventional covalent polymers offers the opportunity to create mechanically robust materials.

Important directions in the field of supramolecular materials include the use of machine learning methodologies to navigate their vast structural and functional space, the use of a "metallurgical" approach to explore the phase diagrams of molecular alloys and discover new functions, and the hybridization of synthetic structures with biomolecular ones that have the advantage of billions of years of evolution to dominantly direct non-covalent association among molecules. Further development of the field of "supramolecular materials" will no doubt offer novel solutions to great societal problems in the areas of sustainable energy, environmental challenges, and transformative changes in human health.

Acknowledgments

We thank R. Shah for providing the previously unpublished scanning electron micrograph shown in Figure 1b and M. Seniw for various illustrations reprinted here.

Author contributions

Not applicable.

Funding

Experimental work in the Stupp laboratory was supported by the US Department of Energy Office of Basic Energy Sciences under Award No. DE-SC002088 (for characterization of PA molecular dynamics and the structure and alloying of PMI chromophore amphiphile supramolecular polymers); the Center for Bio-Inspired Energy Science, an Energy Frontier Research Center funded by the US Department of Energy, Office of Science, Basic Energy Sciences, under Award No. DE-SC0000989 (for photocatalytic and soft robotic materials and for supramolecular bundles); the National Science Foundation under Award No. NSF DMR-1508731 (for the hybrid bonding polymers); and the Center for Regenerative Nanomedicine at the Simpson Querrey Institute for BioNanotechnology (for biological studies).

Data availability

Not applicable.

Code availability

Not applicable.

Conflict of interest

Not applicable.

References

1. S.I. Stupp, V. LeBonheur, K. Walker, L.S. Li, K.E. Huggins, M. Keser, A. Amstutz, *Science* **276**, 384 (1997)
2. M. Sayar, S.I. Stupp, *Macromolecules* **34**, 7135 (2001)
3. M.U. Pralle, K. Urayama, G.N. Tew, D. Neher, G. Wegner, S.I. Stupp, *Angew. Chem. Int. Ed.* **39**, 1486 (2000)
4. R.M. Capito, H.S. Azevedo, Y.S. Velichko, A. Mata, S.I. Stupp, *Science* **319**, 1812 (2008)
5. R.H. Zha, S. Sur, S.I. Stupp, *Adv. Healthc. Mater.* **2**, 126 (2013)
6. D. Carvajal, R. Bitton, J.R. Mantei, Y.S. Velichko, S.I. Stupp, K.R. Shull, *Soft Matter* **6**, 1816 (2010)
7. Y.S. Velichko, J.R. Mantei, R. Bitton, D. Carvajal, K.R. Shull, S.I. Stupp, *Adv. Funct. Mater.* **22**, 369 (2012)
8. H. Okamoto, T. Mitani, Y. Tokura, S. Koshihara, T. Komatsu, Y. Iwasa, T. Koda, G. Saito, *Phys. Rev. B* **43**, 8224 (1991)
9. A.S. Tayi, A.K. Shveyd, A.C.H. Sue, J.M. Szarko, B.S. Rolczynski, D. Cao, T.J. Kennedy, A.A. Sarjeant, C.L. Stern, W.F. Paxton, W. Wu, S.K. Dey, A.C. Fahrenbach, J.R. Guest, H. Mohseni, L.X. Chen, K.L. Wang, J.F. Stoddart, S.I. Stupp, *Nature* **488**, 485 (2012)
10. A.K. Blackburn, A.C.H. Sue, A.K. Shveyd, D. Cao, A. Tayi, A. Narayanan, B.S. Rolczynski, J.M. Szarko, O.A. Bozdemir, R. Wakabayashi, J.A. Lehrman, B. Kahr, L.X. Chen, M.S. Nassar, S.I. Stupp, J.F. Stoddart, *J. Am. Chem. Soc.* **136**, 17224 (2014)
11. A. Narayanan, D. Cao, L. Frazer, A.S. Tayi, A.K. Blackburn, A.C.H. Sue, J.B. Ketterson, J.F. Stoddart, S.I. Stupp, *J. Am. Chem. Soc.* **139**, 9186 (2017)
12. P.K. Nayak, S. Mahesh, H.J. Snaith, D. Cahen, *Nat. Rev. Mater.* **4**, 269 (2019)
13. J.V. Passarelli, D.J. Fairfield, N.A. Sather, M.P. Hendricks, H. Sai, C.L. Stern, S.I. Stupp, *J. Am. Chem. Soc.* **140**, 7313 (2018)
14. J.V. Passarelli, C.M. Mauck, S.W. Winslow, C.F. Perkinson, J.C. Bard, H. Sai, K.W. Williams, A. Narayanan, D.J. Fairfield, M.P. Hendricks, W.A. Tisdale, S.I. Stupp, *Nat. Chem.* **12**, 672 (2020)
15. A.S. Weingarten, R.V. Kazantsev, L.C. Palmer, M. McClendon, A.R. Koltonow, A.P.S. Samuel, D.J. Kiebala, M.R. Wasielewski, S.I. Stupp, *Nat. Chem.* **6**(11), 964 (2014)
16. B. Harutyunyan, A. Dannenhoffer, S. Kewalramani, T. Aytun, D.J. Fairfield, S.I. Stupp, M.J. Bedzyk, *J. Phys. Chem. C* **121**, 1047 (2017)
17. N.J. Hestand, R.V. Kazantsev, A.S. Weingarten, L.C. Palmer, S.I. Stupp, F.C. Spano, *J. Am. Chem. Soc.* **138**(16), 11762 (2016)
18. F.B. Tantakitti, X. Wang, R.V. Kazantsev, T. Yu, J. Li, E. Zhuang, R. Zandi, J.H. Ortony, C.J. Newcomb, L.C. Palmer, G.S. Shekhawat, M. Olvera de la Cruz, G.C. Schatz, S.I. Stupp, *Nat. Mater.* **15**, 469 (2016)
19. A.J. Dannenhoffer, H. Sai, B. Harutyunyan, A. Narayanan, N.E. Powers-Riggs, A.N. Edelbrock, J.V. Passarelli, S.J. Weigand, M.R. Wasielewski, M.J. Bedzyk, L.C. Palmer, S.I. Stupp, *Nano Lett.* **21**, 3745 (2021)
20. A.S. Weingarten, R.V. Kazantsev, L.C. Palmer, D.J. Fairfield, A.R. Koltonow, S.I. Stupp, *J. Am. Chem. Soc.* **137**, 15241 (2015)
21. A.S. Weingarten, A.J. Dannenhoffer, R.V. Kazantsev, H. Sai, D. Huang, S.I. Stupp, *J. Am. Chem. Soc.* **140**, 4965 (2018)
22. R.V. Kazantsev, A. Dannenhoffer, T. Aytun, B. Harutyunyan, D.J. Fairfield, M.J. Bedzyk, S.I. Stupp, *Chem* **4**, 1596 (2018)
23. A. Dannenhoffer, H. Sai, E.P. Bruckner, L. Đorđević, A. Narayanan, Y. Yang, X. Ma, L.C. Palmer, S.I. Stupp, *Chem* **9**, 170 (2023)
24. H. Sai, G.C. Lau, A.J. Dannenhoffer, S.M. Chin, L. Đorđević, S.I. Stupp, *Nano Lett.* **20**, 4234 (2020)
25. S.I. Stupp, T.D. Clemons, J.K. Carrow, H. Sai, L.C. Palmer, *Isr. J. Chem.* **60**, 124 (2020)
26. E.P. Bruckner, T. Curk, L. Đorđević, Z.W. Wang, Y. Yang, R.M. Qiu, A.J. Dannehoffer, H. Sai, J. Kupferberg, L.C. Palmer, E. Lujiten, S.I. Stupp, *ACS Nano* **16**, 8993 (2022)
27. C. Li, A. Iscen, L.C. Palmer, G.C. Schatz, S.I. Stupp, *J. Am. Chem. Soc.* **142**, 8447 (2020)
28. J.D. Hartgerink, E. Beniash, S.I. Stupp, *Science* **294**, 1684 (2001)
29. Z. Álvarez, A.N. Kolberg-Edelbrock, I.R. Sasselli, J.A. Ortega, R. Qiu, Z. Syrgiannis, P.A. Mirau, F. Chen, S.M. Chin, S. Weigand, E. Kiskinis, S.I. Stupp, *Science* **374**, 848 (2021)
30. V.M. Tysseling-Mattiace, V. Sahni, K.L. Niece, D. Birch, C. Czeisler, M.G. Fehlings, S.I. Stupp, J.A. Kessler, *J. Neurosci.* **28**, 3814 (2008)
31. R.N. Shah, N.A. Shah, M.M. Del Rosario Lim, C. Hsieh, G. Nuber, S.I. Stupp, *Proc. Natl. Acad. Sci. U.S.A.* **107**, 3293 (2010)
32. S.S. Lee, E.L. Hsu, M. Mendoza, J. Ghodasra, M.S. Nickoli, A. Ashtekar, M. Polavarapu, J. Babu, R.M. Riaz, J.D. Nicolas, D. Nelson, S.Z. Hashmi, S.R. Kaltz, J.S. Earhart, B.R. Merk, J.S. McKee, S.F. Bairstow, R.N. Shah, W.K. Hsu, S.I. Stupp, *Adv. Healthc. Mater.* **4**, 131 (2015)
33. M.J. Webber, J. Tongers, C.J. Newcomb, K.-T. Marquardt, J. Bauersachs, D.W. Losordo, S.I. Stupp, *Proc. Natl. Acad. Sci. U.S.A.* **108**, 13438 (2011)
34. Z. Álvarez, J.A. Ortega, K. Sato, I.R. Sasselli, A.N. Kolberg-Edelbrock, R. Qiu, K.A. Marshall, T.P. Nguyen, C.S. Smith, K.A. Quinlan, V. Papakis, Z. Syrgiannis, N.A. Sather, C. Musumeci, E. Engel, S.I. Stupp, E. Kiskinis, *Cell Stem Cell* **30**, 219 (2023)
35. M.H. Sangji, H. Sai, S.M. Chin, S.R. Lee, I.R. Sasselli, L.C. Palmer, S.I. Stupp, *Nano Lett.* **21**, 6146 (2021)
36. J.H. Ortony, C.J. Newcomb, J.B. Matson, L.C. Palmer, P.E. Doan, B.M. Hoffman, S.I. Stupp, *Nat. Mater.* **13**, 812 (2014)
37. J.H. Ortony, B. Qiao, C.J. Newcomb, T.J. Keller, L.C. Palmer, E. Deiss-Yehiely, M. Olvera de la Cruz, S. Han, S.I. Stupp, *J. Am. Chem. Soc.* **139**, 8915 (2017)

38. R. Freeman, M. Han, Z. Álvarez, J.A. Lewis, J.R. Wester, N. Stephanopoulos, M.T. McClendon, C. Lynsky, J.M. Godbe, H. Sangji, E. Luijten, S.I. Stupp, *Science* **362**, 6141 (2018)
39. J.R. Wester, J.A. Lewis, R. Freeman, H. Sai, L.C. Palmer, S.E. Henrich, S.I. Stupp, *J. Am. Chem. Soc.* **142**, 12216 (2020)
40. A.N. Edelbrock, T.D. Clemons, S.M. Chin, J.J.W. Roan, E.P. Bruckner, Z. Álvarez, J.F. Edelbrock, K.S. Wek, S.I. Stupp, *Adv. Sci.* **14**, 2004042 (2021)
41. R.Z. Pavlović, S.A. Egner, L.C. Palmer, S.I. Stupp, *J. Polym. Sci.* **61**, 870 (2023) □

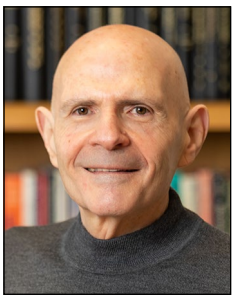

Samuel I. Stupp is Board of Trustees Professor of Materials Science and Engineering, Chemistry, Medicine, and Biomedical Engineering at Northwestern University. He also directs at Northwestern the Simpson Querrey Institute for BioNanotechnology, the Center for Regenerative Nanomedicine, and the Center for Bio-Inspired Energy Science. His research is focused on raising the bar on autonomous self-assembly of molecules, supramolecular chemistry, and the development of bioactive biomaterials and energy materials to solve important societal problems. Stupp can be reached by email at s-stupp@northwestern.edu.

Liam C. Palmer is currently a research professor in the Department of Chemistry and the director of Research for the Simpson Querrey Institute for BioNanotechnology at Northwestern University. He earned his BS degree in chemistry from the University of South Carolina and his PhD degree from The Scripps Research Institute. Palmer can be reached by email at liam-palmer@northwestern.edu.